LANGMUIR

pubs.acs.org/Langmuir Article

Molecular Dynamics Study of Bubble Nucleation on an Ideally Smooth Substrate

Yu-Jie Chen, Xue-Jiao Chen, Bo Yu,* Yu Zou, and Wen-Quan Tao

Cite This: Langmuir 2020, 36, 13725−13734 Read Online

ACCESS | Metrics & More | Article Recommendations

ABSTRACT: Questions regarding bubble nucleation on an ideally smooth surface are seemingly endless, but it can not be adequately verified yet because of the scale limitation (microscopic scale). Hence, in this study, bubble nucleation on an ideally smooth substrate is explored using the molecular dynamics simulation method. An ideally smooth hydrophilic platinum substrate at 145 K is conducted to heat the simple L−J liquid argon. Results show that a visible bubble nucleus successfully forms on the ideally smooth substrate without any additional disturbance, which is common in boiling studies using the traditional numerical simulation methods. However, the nucleation position is unpredictable. At the atomic level, the thermal energy transfer from an ideally smooth substrate to liquid atoms is inhomogeneous due to atomic inhomogeneous distribution and irregular movement, which are the key influencing factors for achieving bubble nucleation. The inhomogeneity will be highlighted with the heating process. As a result, some local liquid atoms near the ideally smooth surface absorb more thermal energy to overcome their potential barrier at a specific moment, causing the emergence of a distinct nucleus there. Furthermore, nanostructure substrates are introduced to make a comparison with the smooth substrate in bubble nucleation. There is no significant difference in the inception temperature of nucleation between the ideally smooth and nanostructure substrates, but the latter has better performance in improving the bubble nucleation rate.

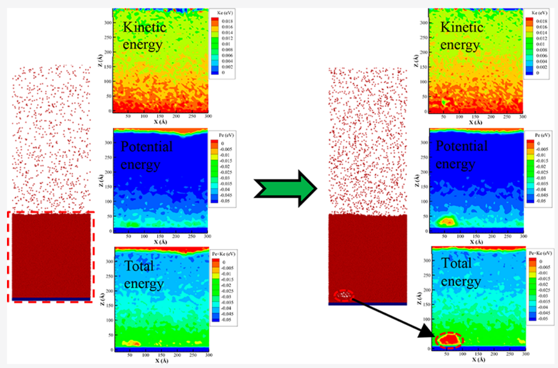

■ INTRODUCTION

Nucleate boiling is perpetually the focus of studies on enhancing heat dissipation due to its high heat transfer efficiency.[1] The experiment is the conventional method to study the influences of wettability, nanostructure, overheating, and cavity on nucleate boiling, but it cannot eliminate the interference of various factors.[2−4] Alternatively, numerical simulation methods are another tool used to study nucleate boiling without the aforementioned drawbacks of the experimental method. However, macroscopic simulation methods, such as VOSET and VOF, require an initial bubble nucleus in the numerical simulation of nucleate boiling, limiting their applications in many fields.[5] The completed process of nucleate boiling, including bubble nucleation, growth, detachment, and coalescence, can be investigated by the mesoscopic lattice Boltzmann method.[6] However, an artificial disturbance is a prerequisite in the nucleate boiling study on an ideally smooth substrate with uniform wettability. Therefore, both macroscopic and mesoscopic methods are unavailable to study the bubble nucleation mechanism on an ideally smooth substrate.

The conventional pre-existing nuclei (PEN) theory suggests that the requirement for nucleation on an ideally smooth substrate is stringent,[7,8] but it cannot be adequately verified because of the scale limitation (microscopic scale). An in-depth investigation of the nucleation mechanism is vital to intensify boiling heat transfer, especially with the development of micro/nanotechnology. Fortunately, the molecular dynamics simulation method (MD) can handle the study of the phase transition behaviors on the microscopic scale, and it has become one of the most prevalent tools for numerical simulation studies.

Extensive studies have been conducted by MD in the phase transition.[7−16] Shavik et al.[10] employed MD to investigate substrate wettability influences on phase transition behaviors. Liquid argon film was heated by an ideally smooth platinum substrate at high and low superheating temperatures, corresponding to explosive boiling and evaporation phenomena, respectively. Besides, explosive boiling happened more quickly when the substrate hydrophilicity was enhanced. Similar studies of explosive boiling and evaporation on an ideally smooth substrate were conducted by Hens et al.[8] and

Received: September 26, 2020
Revised: October 28, 2020
Published: November 4, 2020

Mao et al.[11] However, only a vapor film occurs without a distinct bubble nucleation process during explosive boiling. For an ideally smooth substrate, if the wettability or superheat is not uniform, the phase transition behavior changes. Yamamoto et al.[7] examined bubble nucleation on a smooth substrate with uneven superheat and wettability, respectively. Some liquid atoms near the region with higher superheat or stronger hydrophilicity obtained more thermal energy than other regions, causing the expansion of local liquid atoms into a bubble nucleus. Hens et al.[8] also investigated boiling on a smooth substrate with a local heater in the center. A bubble nucleus was observed in the central region, and the nucleation inception was shortened with the improvement in hydrophilicity because it facilitated the heat transfer to the liquid. Utilizing a smooth surface with inhomogeneous wettability, Zhou et al.[12] investigated superheat influences on bubble nucleation. It was attractive that the bubble nucleation position changed with the substrate superheat. The bubble nucleus occurred on the hydrophobic part at a low superheat, and it changed to the hydrophilic part with the increasing superheat. When the substrate temperature was increased up to a specific value, the bubble nucleus appeared on hydrophobic and hydrophilic parts simultaneously. It was noteworthy that the results of Yamamoto et al.[7] were different from those of Zhou et al.[12] because only a high heating temperature was adopted in the former study.

Nanostructure is another available selection to achieve bubble nucleation. Mukherjee et al.[13] studied bubble nucleation on a grooved surface using MD. The energy of liquid atoms near the groove increased quickly when a constant heat flux was applied. As a result, these liquid atoms converted into a bubble nucleus. Zhang et al.[14] also explored the bubble nucleation phenomena on a grooved substrate. Simulation results indicated that the substrate wettability significantly affected the bubble nucleation and the heat exchange at the solid−liquid interface. The heat transfer and bubble nucleation were promoted by properly increasing the substrate hydrophilicity, and the conclusions were similar to those of Hens.[8] Chen et al.[15] employed a hydrophilic convex nanostructure to enhance bubble nucleation efficiency. The convex nanostructure was favorable for bubble nucleation because it provided greater exchange area of thermal energy. However, the nanostructure morphology had no significant influence on bubble nucleation when both the height and the surface area of convex nanostructures were unified. Alternatively, Chen et al.[16] also investigated groove influences on bubble nucleation. The groove affected bubble nucleation from two aspects: it provided an initial nucleus and enhanced thermal energy exchange. At the beginning of the nonequilibrium heating stage, some gases remained in the hydrophobic groove to become an initial bubble nucleus. Nevertheless, this nucleus needed some time to mature. For a hydrophilic groove, a bubble nucleus emerged from nothing because it provided a large heat exchange area. Besides, some bubble nucleation studies were conducted in a nanochannel with different nanostructures. Liu et al.[17] compared free energy changes during the nanobubble formations inside a nanochannel with different roughnesses. Results showed that moderate roughness was favorable for the formation of a stable nanobubble. She et al.[18] studied the groove influences on forming a bubble nucleus in a nanochannel. The groove reduced the relative density of argon and promoted the formation of a large bubble nucleus. However, no bubble nucleus formed when the nanochannel was strongly hydrophobic.

At the nanoscale, significant insights into bubble nucleation have been provided from the above studies. The inhomogeneities of overheat, wettability, and nanostructure have substantial impacts on bubble nucleation. However, the feasibility of bubble nucleation on an ideally smooth surface with homogeneous hydrophilicity in a system with a free liquid−vapor surface has not yet been explicitly revealed. Nagayama et al.[19] explored bubble nucleation in an ideally smooth nanochannel. A nanosized bubble nucleus was observed under different wettability conditions. However, the unsaturated liquid was the precondition for bubble nucleation in the nanochannel. Besides, the height of the nanochannel was fixed, leading to a fixed bubble nucleus size in the final. These problems are hard to be solved for the nanochannel system. At the atomic level, the movement and distribution of atoms are nonuniform. These inhomogeneities for the liquid atoms on an ideally smooth substrate in a system with a free liquid−vapor surface will be highlighted during the heating process, which may finally lead to the emergence of a bubble nucleus. Therefore, on an ideally smooth substrate with homogeneous hydrophilicity, the bubble nucleation is investigated by the molecular dynamics simulation method in this study. The intrinsic mechanism for that is thoroughly investigated by the interatomic interaction and atomic irregular movement. Moreover, further comparisons in nucleation behaviors are made between the ideally smooth and nanostructure substrates.

■ SIMULATION SYSTEM AND METHOD

As shown in Figure 1, liquid argon (Ar) is chosen as the study object for bubble nucleation, and the metal platinum (Pt) substrate acts as the heat source with a Langevin thermostat in the present study. At the bottom of the simulation box, more than 12 000 metal platinum atoms are placed there with face-centered cubic lattice (FCC (1 1 1)), and 97 000 liquid atoms with a density of 1367 kg/m^3 are arranged on the platinum surface. Some liquid argon atoms at the free surface evaporate into the upper region and become vapor atoms during the equilibrium simulation process. In the present study, the bubble nucleation is investigated based on three types of substrates: ideally smooth substrate, convex nanostructure substrate, and grooved substrate, as shown in Figure 2 (front view). These substrates serve as the heat source in the nonequilibrium simulation stage, and their configurations are illustrated in Table 1. On the aspect of boundary conditions, the reflecting wall and periodic boundary are applied to

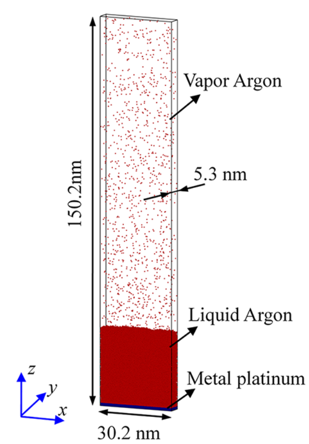

Figure 1. Initial configurations of the simulation system.

Figure 2. Different substrates for the investigation of bubble nucleation: (a) ideally smooth substrate, (b) grooved substrate, and (c) convex nanostructure substrate.

Table 1. Configurations of Different Substrates

substrate type	length of substrate (nm)	width of substrate (nm)	width of nanostructure (nm)	height/depth of nanostructure (nm)
smooth substrate	30.2	5.0		
grooved substrate	30.2	5.0	5.2	2.9
convex nanostructure substrate	30.2	5.0	5.2	4.5

the vertical direction (z-direction) and horizontal directions (x- and y-directions), respectively.[7−12]

The potential calculation is a crucial step in MD simulation. In this study, a common Lennard−Jones (L−J) potential is used to describe Ar−Ar, Ar−Pt, and Pt−Pt interactions.

$$\phi_{Ar-Ar}(r) = 4\varepsilon_{Ar-Ar}\left[\left(\frac{\sigma_{Ar-Ar}}{r}\right)^{12} - \left(\frac{\sigma_{Ar-Ar}}{r}\right)^{6}\right] \quad (1)$$

$$\phi_{Pt-Pt}(r) = 4\varepsilon_{Pt-Pt}\left[\left(\frac{\sigma_{Pt-Pt}}{r}\right)^{12} - \left(\frac{\sigma_{Pt-Pt}}{r}\right)^{6}\right] \quad (2)$$

$$\phi_{Pt-Ar}(r) = 4\varepsilon_{Pt-Ar}\left[\left(\frac{\sigma_{Pt-Ar}}{r}\right)^{12} - \left(\frac{\sigma_{Pt-Ar}}{r}\right)^{6}\right] \quad (3)$$

$$\sigma_{Pt-Ar} = \frac{\sigma_{Pt} + \sigma_{Ar}}{2} \quad (4)$$

$$\varepsilon_{Pt-Ar} = \sqrt{\varepsilon_{Pt}\varepsilon_{Ar}} \quad (5)$$

where σ and ε represent the length parameter and the energy parameter, respectively, and the Lorentz−Berthelot combining rule[20] is conducted to obtain them for Pt−Ar. The L−J parameters for different types of interactions are shown in Table 2.

Table 2. Lennard−Jones Parameters for Ar−Ar, Ar−Pt, and Pt−Pt Interactions[9]

interaction type	ε (eV)	σ (nm)
Ar−Ar	0.0104	0.3405
Pt−Pt	0.5219	0.2475
Pt−Ar	0.0737	0.2940

In this study, the microcosmic phase transition processes of a liquid film on different substrates are simulated by an open-source simulator LAMMPS.[21] The simulation includes two procedures: first, based on the canonical ensemble (NVT), a stable system at 90 K is reached through a 2.5 ns equilibrium simulation; then, after increasing the substrate temperature up to 145 K, a nonequilibrium simulation is respectively employed to investigate the phase transition phenomena on the ideally smooth and nanostructure substrates in the microcanonical ensemble (NVE). During the simulation process, atomic velocity and position are updated every 5 fs by a Velocity-Verlet algorithm, and the corresponding results are visualized by the open software OVITO.[22]

■ RESULTS AND DISCUSSION

In this section, the feasibility of bubble nucleation on an ideally smooth substrate is illustrated. Moreover, comparisons in nucleation temperature and nucleation rate are made between the ideally smooth and nanostructure substrates.

Feasibility of Bubble Nucleation on an Ideally Smooth Substrate. To improve the reliability of the numerical simulation results of bubble nucleation on an ideally smooth substrate, three repeated nonequilibrium simulations of bubble nucleation processes are conducted in this subsection. After equilibrium simulation, additional simulations with a few time steps are required to obtain different initial configurations of simulation systems for the repeated nonequilibrium simulations. Figure 3 shows the representative snapshots of the bubble nucleation processes of argon film on ideally smooth hydrophilic substrates. For these three cases with different initial configurations, a distinct bubble nucleus appears on the ideally smooth substrate at 5900, 6000, and 6200 ps, respectively, indicating that bubble nucleation can happen on the ideally smooth substrate without any nanostructure, pre-existing nucleus, or artificial disturbance. Different initial configurations cause a slight difference in the incipient nucleation time. Besides, the needed overheat for bubble nucleation on the smooth substrate is not significantly higher than that on the nanostructure substrate, which will be illustrated in the next subsection. However, the bubble nucleation position is unexpected but also relates to the initial configurations because the Velocity-Verlet algorithm determines the atomic position at every step during the nonequilibrium stage. Next, the first case (Smooth substrate A) with the incipient nucleation time of 5900 ps is selected as the representative to reveal the intrinsic mechanism for bubble nucleation on an ideally smooth substrate.

In this study, the study object is the simple L−J liquid argon with only Van Der Waals interaction. Each liquid atom possesses potential energy and kinetic energy only.[16] Liquid atom evaporation from the liquid−vapor interface can be considered as an escape from the potential well,[23] and the impetus for this escape is its kinetic energy. Similarly, the bubble nucleation mechanism on an ideally smooth substrate can be illustrated from the perspective of the competition between the kinetic energy and potential energy of liquid atoms ("PK" norm).[16] Therefore, the subsequent analysis focuses on whether the potential barrier and the obtained kinetic energy of liquid atoms are uniform or not in different regions. If not, then some local liquid atoms will absorb enough kinetic energy to overcome their potential barrier first, and the bubble nucleus is forming in there. The method for obtaining the contours of atomic potential energy and atomic kinetic energy during the simulation process is referred to in ref 16. It is noteworthy that the energy value of each point in the contour is calculated every 100 time-steps and averaged every 1000 time-steps.

https://dx.doi.org/10.1021/acs.langmuir.0c02832
Langmuir 2020, 36, 13725−13734

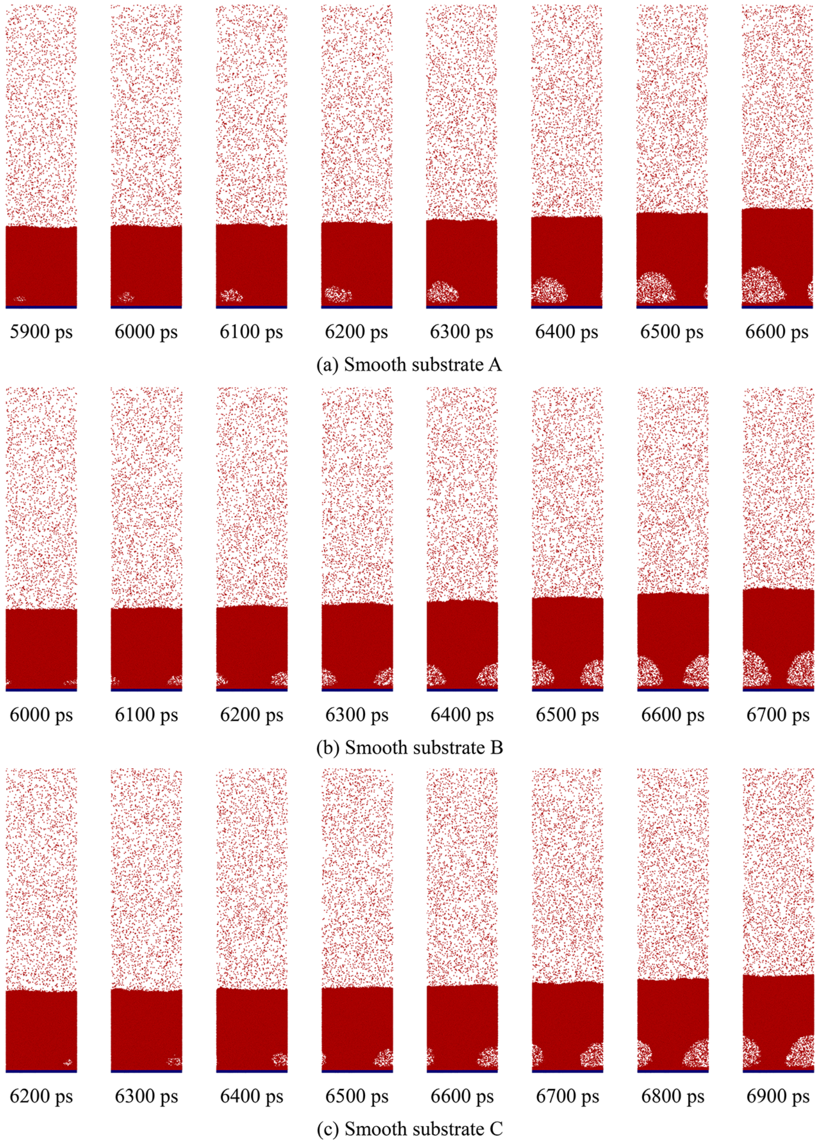

Figure 3. Representative snapshots of bubble nucleation processes on (a) smooth substrate A, (b) smooth substrate B, and (c) smooth substrate C.

Figure 4 shows the contour of the atom number at 2500 ps. $z = 0$ Å is the liquid−solid interface, and 2500 ps is the final moment of the equilibrium stage. The atomic distribution is not entirely uniform at 2500 ps, and utterly uniform atomic distribution is impossible in MD study and real liquids. However, the atomic distribution affects the changes in both potential energy and kinetic energy. The potential barrier is related to the interatomic interaction and atomic distribution, and nonuniform atomic distribution causes different potential barriers for each liquid atom at 2500 ps. Besides, the kinetic energy exchange between different atoms is by means of "collision" (one atom cannot entirely collide with another atom because of the L−J potential between them), which is also decided by the atomic distribution. The "collision" probability decreases with the increasing atomic distance. Therefore, heat transfer from the substrate to liquid is not uniform during the nonequilibrium simulation stage as well. These inhomogeneities play vital roles in bubble nucleation and cause the difference among these three smooth cases with different initial configurations in the nucleation time.

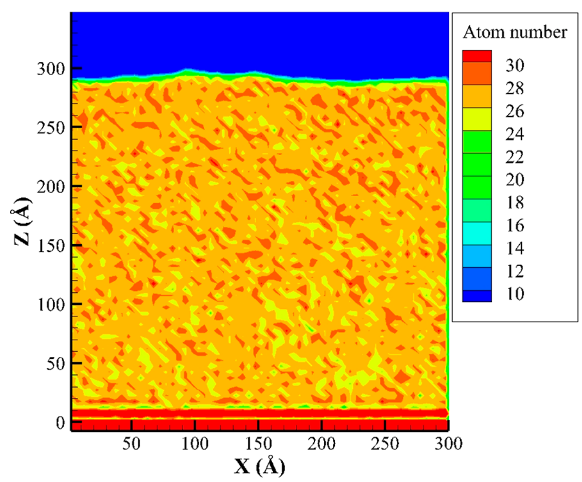

Figure 4. Distributions of atom number in the case with an ideally smooth substrate at 2500 ps.

Energy contours in the case with an ideally smooth substrate at 4000 ps are shown in Figure 5. Under the effect of the

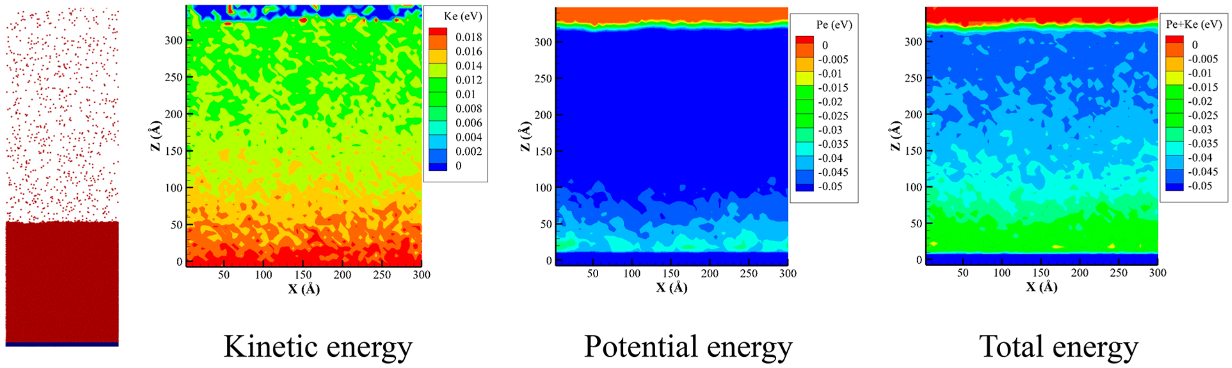

Figure 5. Kinetic energy, potential energy, and total energy contours in the case with an ideally smooth substrate at 4000 ps.

nonuniform atomic distribution, although liquid atoms near the ideally smooth substrate absorb thermal energy synchronously, the changes of kinetic energy and potential energy are different in different liquid regions. It is worth stressing that a part of the thermal energy transforms into atomic kinetic energy, and the others transform into atomic potential energy.[16] The potential energy is a negative value, indicating a limitation on the phase transition of liquid atoms. The increasing potential energy means the weakening of the potential barrier for bubble nucleation.[16] At 4000 ps, the kinetic energy of liquid atoms is still weaker than their potential barrier, and no bubble nucleus appears inside the liquid at that moment, as shown in Figure 5. Even so, as shown in Figure 6, the inhomogeneity of the atomic distribution is

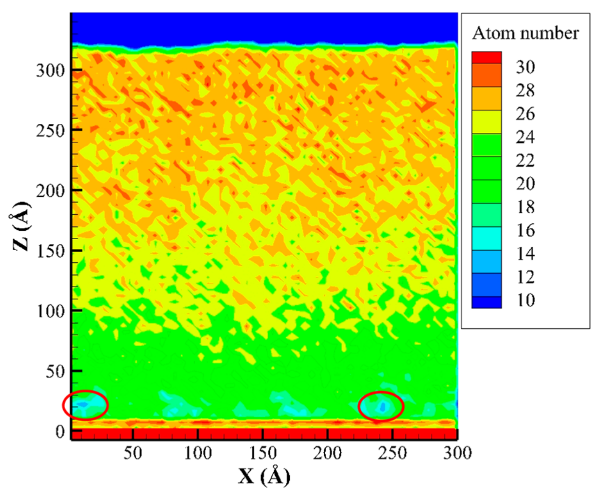

Figure 6. Distributions of atom number in the case with an ideally smooth substrate at 4000 ps.

enlarged under the effect of asynchronous energy change in the liquid region before 4000 ps, especially for the region near the substrate. The density fluctuation of liquid atoms is in favor of bubble nucleation.

With the increasing time, more thermal energy from the heat source is transferred to liquid atoms to weaken their potential barrier and increase their kinetic energy.[16] Certainly, the evolution of atomic energy still is irregular, which is favorable for achieving bubble nucleation. However, the nucleation position is difficult to predict until the inhomogeneity of the obtained energy is highlighted. As shown in Figure 7(a), at 5700 ps, above the right side of the smooth substrate, the potential barrier of the local liquid atoms is obviously weaker than surrounding atoms, and the total energy in there is closed to 0 eV. Therefore, some liquid atoms in there are going to overcome their potential barrier after 5700 ps. As expected, at about 5900 ps, some liquid atoms with high kinetic energy in this region overcome their potential barrier and become activated atoms, as shown in Figure 7(b), leading to the emergence of a bubble nucleus on the ideally smooth substrate. After forming the bubble nucleus, at the bubble nucleus interface, the potential barrier of liquid atoms decreases quickly because of the considerable interatomic distance inside the bubble nucleus.[16] As a result, a large number of liquid atoms with high kinetic energy at the bubble nucleus interface overcome their weak potential barrier and evaporate into the bubble nucleus, leading to its growth, as shown in Figure 7(c). Besides, some researchers have proposed that a vapor bubble grows because of the evaporation at the bubble interface,[24] and the surrounding superheated liquid layer supplied the energy for evaporation. This opinion is consistent with our explanation.

Stefanović and Novaković[1,25,26] used an ideally smooth substrate to exclude the effects of substrate roughness elements, which favored breeding an initial bubble nucleus according to the PEN theory. The ideally smooth substrate was obtained by heating a layer of mercury, which was distilled to eliminate any impurities and air. The results indicated that the sites of bubble nucleation on the smooth mercury surface were similar to that on a rough solid surface, but the bubble nucleation sites on the ideally smooth mercury surface exhibited irregular motion. On the basis of these findings, Stefanović and Novaković concluded that the effect of gas entrapment in substrate cavities on bubble nucleation was overestimated by the PEN theory.[1] The experimental results indicate that the bubble nucleation can happen on an ideally smooth surface with homogeneous wettability, coinciding with the present simulation results.

In summary, the bubble nucleus successfully forms on an ideally smooth substrate with uniform hydrophilicity, and the initial inhomogeneity of atomic distribution is the chief reason for that. The initial inhomogeneity is enlarged with the heating process, leading to unfair competition between potential energy and kinetic energy in different liquid regions. Therefore, some local liquid atoms near the ideally smooth substrate obtain enough kinetic energy to overcome the potential barrier and achieve nucleation first.

Comparisons between Ideally Smooth and Nanostructure Substrates on Bubble Nucleation. Stefanović and Novaković[1,25,26] also found that the overheat measured during boiling did not show a significant difference from those

https://dx.doi.org/10.1021/acs.langmuir.0c02832
Langmuir 2020, 36, 13725−13734

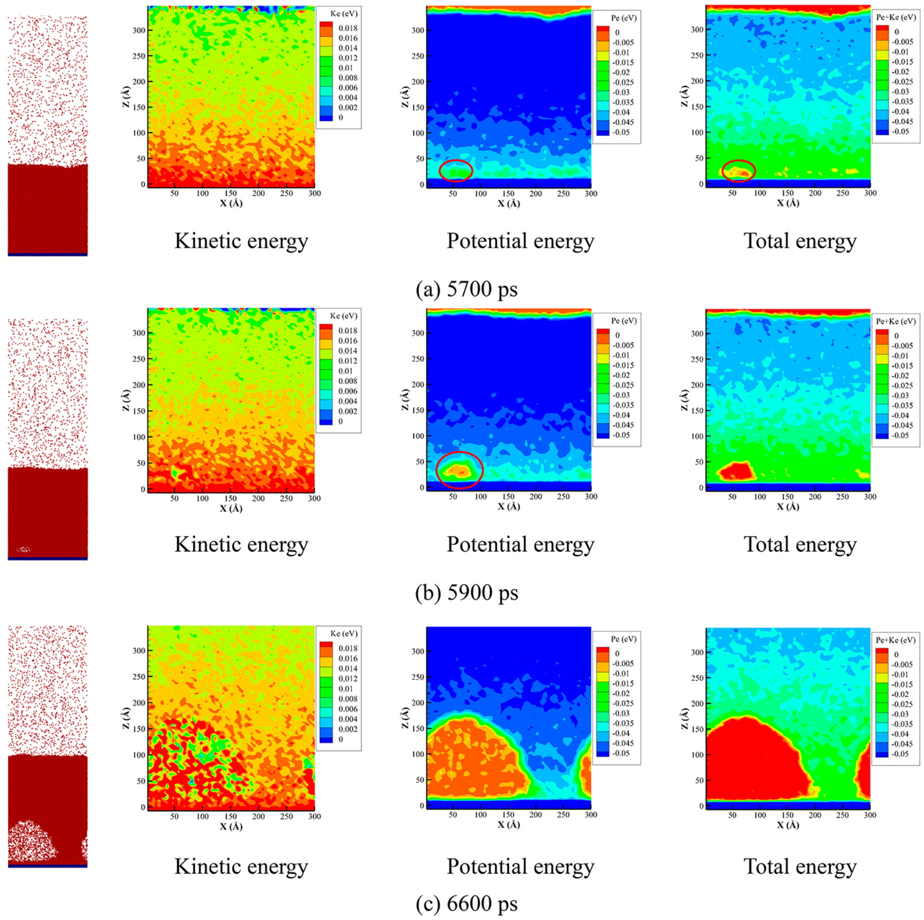

Figure 7. Kinetic energy, potential energy, and total energy contours in the cases with an ideally smooth substrate at (a) 5700 ps, (b) 5900 ps, and (c) 6600 ps.

observed on a rough solid substrate. Therefore, in this subsection, the differences in nucleation position, nucleation temperature, and nucleation rate between ideally smooth and nanostructure substrates are investigated further to promote the comprehension of the bubble nucleation at the nanoscale. The nanostructure substrates include two types: grooved substrate and convex nanostructure substrate.

Figure 8 shows the bubble nucleation processes of argon film on the different nanostructure substrates. Only one distinct bubble nucleus emerges on the groove region for the case with a grooved substrate at about 5100 ps. There is no vapor embryo in the grooved substrate, whose surface is covered by a layer of liquid atoms all along. Bankoff et al.[27] provided a criterion for gas entrapment in a groove that the grooved angle should be bigger than the contact angle. Obviously, in this study, the grooved substrate does not satisfy the precondition because its wettability is strongly hydrophilic. In the case with a convex nanostructure substrate, one bubble nucleus forms on the right side of the nanostructure at about 4650 ps, and another one appears on the left side of the nanostructure at about 5050 ps. The reason for the asynchronous nucleation processes of these two bubble nuclei on the convex nanostructure substrate will be illustrated in the next part. The inception of nucleation on nanostructure substrates is much earlier than that on the ideally smooth substrate (the average incipient nucleation time is 6033 ps). Moreover, the nucleation position is specific on the nanostructure substrates under the effect of nanostructures, which is different from the smooth substrate. Besides, the nucleation position in all cases is not clinging to the substrate surface in this study. At the atomic level, the reason for that is the liquid atoms adhering to the hydrophilic substrate surface suffer a strong potential barrier from it, which they cannot break.[16]

Then, the differences in nucleation position and nucleation time between the nanostructure and the smooth substrates are explained by the competition between the kinetic energy and the potential barrier of liquid atoms during the nonequilibrium simulation stage. Figure 9 shows energy contours in the case with a grooved substrate at 4000 and 5100 ps, respectively. There is no significant difference in kinetic energy contour between the ideally smooth substrate and the grooved substrate at 4000 ps. However, different from the smooth substrate, both the total energy and the potential energy of liquid atoms in the groove region are higher than those of the surrounding smooth regions, indicating that a large proportion of the absorbed energy of liquid atoms transforms into their potential energy there, as shown in Figure 9(a). Obviously, the groove dominates the inhomogeneity of the liquid energy distribution in the vicinity of the substrate, and the inhomogeneity is highlighted more quickly and easily than the ideally smooth substrate. As time goes on, because of the large exchange area of the groove, more and more thermal energy is transformed to weaken the potential barrier of liquid atoms there. As a result, as shown in Figure 9(b), a distinct bubble nucleus appears on the central groove at about 5100 ps,

https://dx.doi.org/10.1021/acs.langmuir.0c02832
Langmuir 2020, 36, 13725−13734

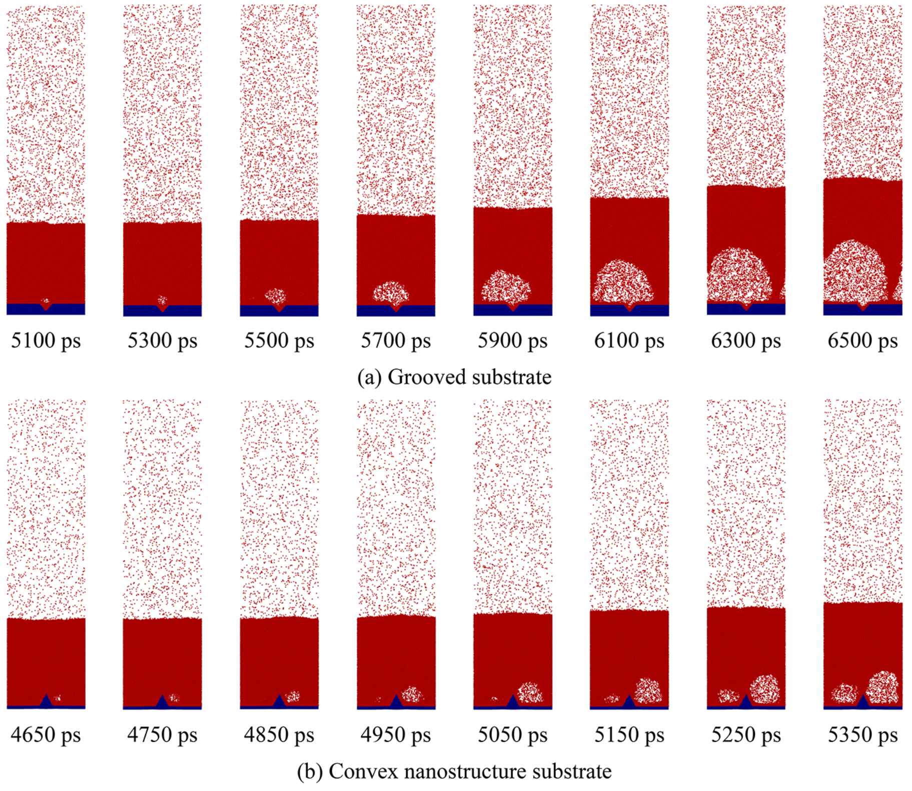

Figure 8. Representative snapshots of bubble nucleation processes on (a) grooved substrate and (b) convex nanostructure substrate.

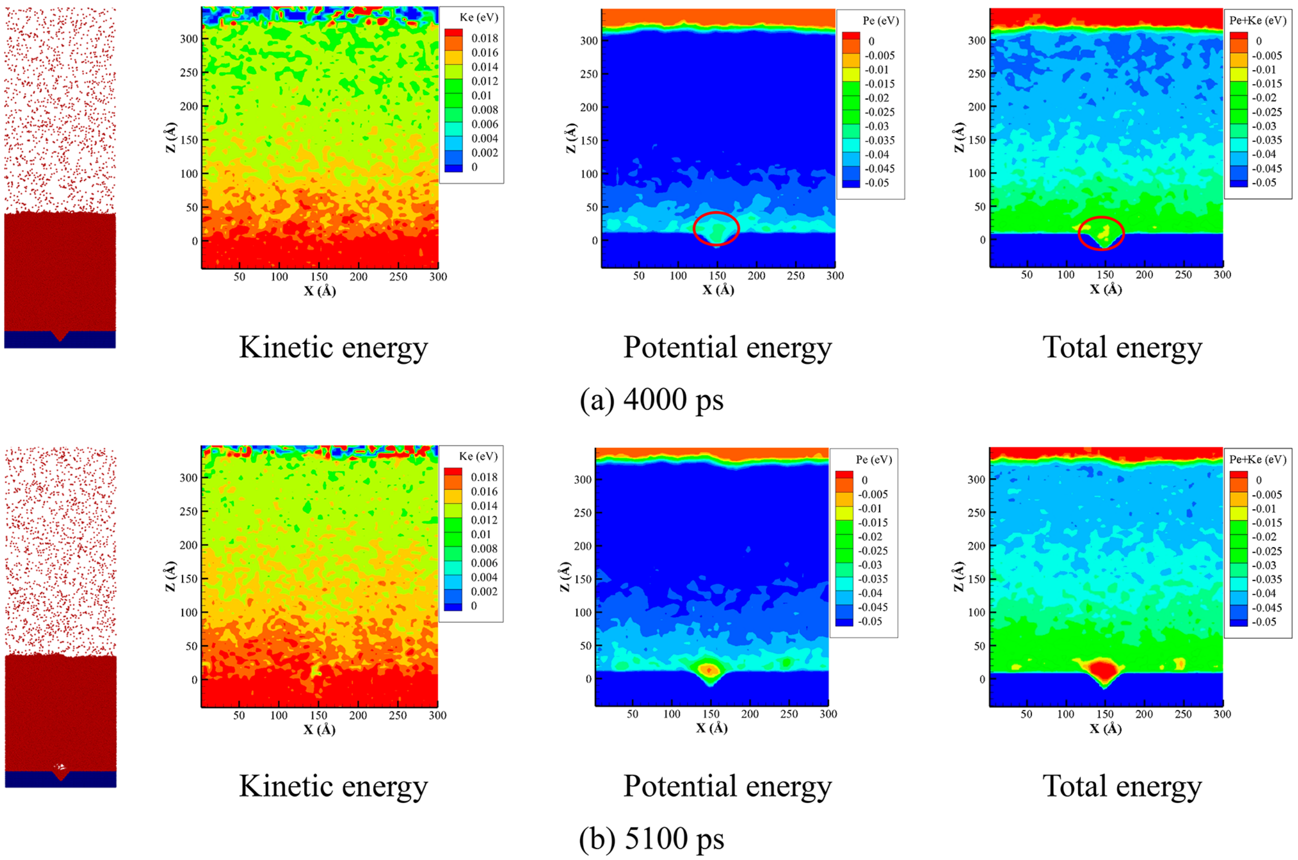

Figure 9. Kinetic energy, potential energy, and total energy contours in the case with a grooved substrate at (a) 4000 ps and (b) 5100 ps.

which is much earlier than the incipient nucleation time of liquid on an ideally smooth substrate.

Figure 10 shows energy contours in the case with a convex nanostructure substrate at 4000 and 4650 ps, respectively. It is

https://dx.doi.org/10.1021/acs.langmuir.0c02832
Langmuir 2020, 36, 13725−13734

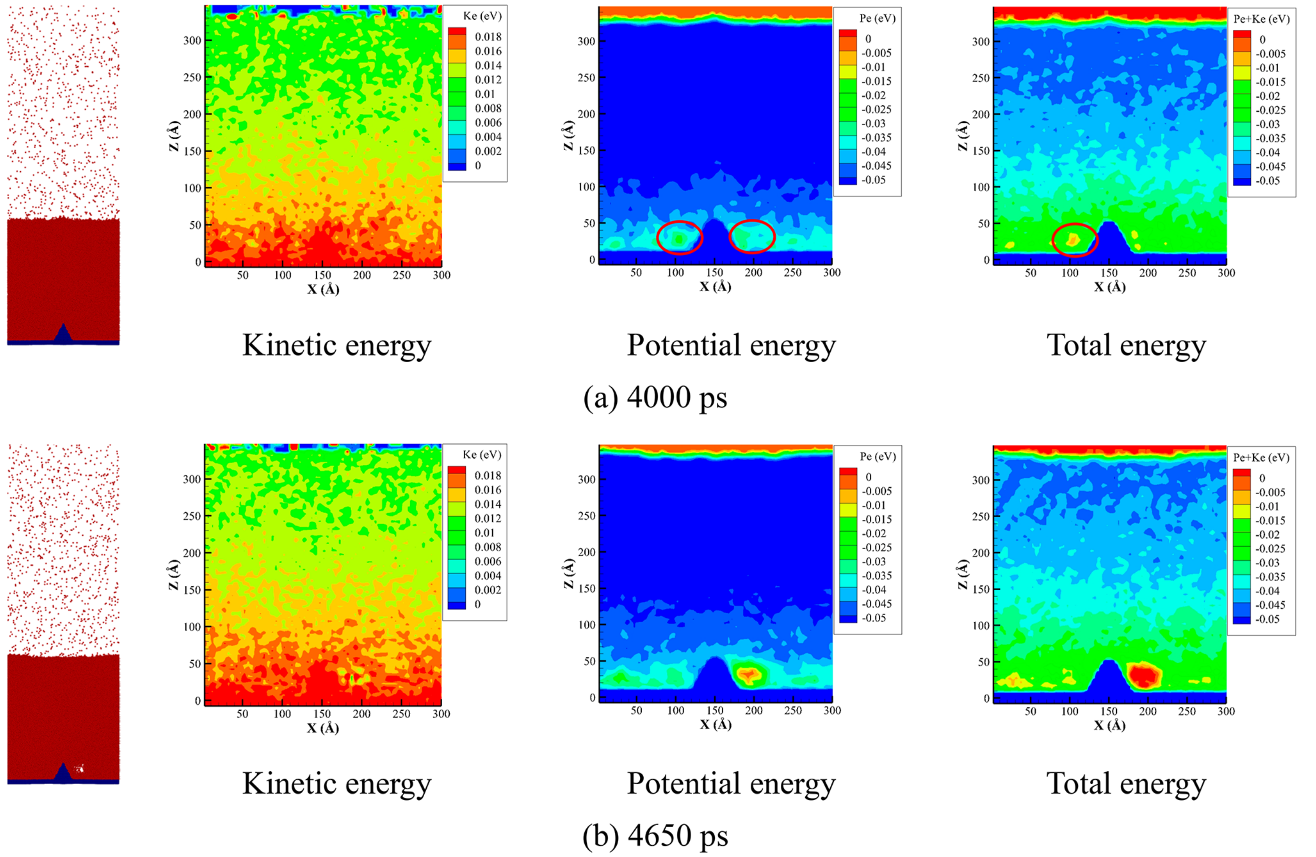

Figure 10. Kinetic energy, potential energy, and total energy contours in the case with a convex nanostructure substrate at (a) 4000 ps and (b) 4650 ps.

found that the atomic energy is not consistent on both sides of the convex nanostructure because of the inhomogeneous distribution and irregular movement of liquid atoms. At 4000 ps, the total energy of the liquid atoms on the left side of the nanostructure is larger than that on the right side, as shown in Figure 10(a). However, with the increasing time, the liquid atoms on the right side of the nanostructure obtain a great deal of thermal energy and exceed that on the left side. Moreover, the liquid atoms on the right side of the nanostructure overcome the potential barrier and nucleate first at about 4650 ps, as shown in Figure 10 (b). Similar to the grooved substrate, the exchange of thermal energy is violent near the nanostructure region, causing the shortening of nucleation time and the certainty of the nucleation position by comparing it with the ideally smooth substrate.

Next, the differences in nucleation temperature and nucleation rate between nanostructure and ideally smooth substrates are illustrated sequentially. On the basis of the region where the potential barrier is weaker than the atomic kinetic energy, the bubble nucleation position is located. Around the nucleation moment, the statistical average temperature in the nucleation position is taken as the approximate nucleation temperature, which is 135.4, 135.7, and 136.3 K for the liquid on the ideally smooth substrate, grooved substrate, and convex nanostructure substrate, respectively. The maximum relative difference in the nucleation temperature of liquid argon between the cases with an ideally smooth substrate and a nanostructure substrate is only 0.67%. Therefore, it is concluded that for the hydrophilic substrate, no significant difference is seen in the nucleation temperature of liquid argon between the ideally smooth and nanostructure substrates considering the statistical error. The result is similar to that of Stefanović and Novaković in that the overheat measured during boiling on a smooth substrate does not show a significant difference from that observed on a rough solid substrate. The reason for this can be illustrated by the potential barrier in the bubble nucleation position. In all simulation cases, the distance between the bubble nucleation position and the substrate surface is more than $3.5\sigma_{Ar}$, which is the cutoff radius of potential calculation, as shown in Figures 7, 9, and 10. Therefore, the substrate geometry has few effects on the initial potential barrier for bubble nucleation in this study. As a result, the needed kinetic energy (temperature) for nucleation on different substrates is approximate. Alternatively, in the macro experiment, there were few entrapped gases in the substrate for well-wetting liquids.[28] The observed inception overheats for well-wetting liquids are much higher than partially wetting liquids.[29] The preexisting vapor nucleus plays a crucial role in the incipient nucleation temperature.[30] However, in the present study, there are no preexisting vapor nuclei for all cases in the initial moment of the nonequilibrium stage, which may be another explanation for the few differences in nucleation temperature from the macro perspective. It is noteworthy that under the same simulation conditions, the obtained bubble nucleation temperature for the hydrophilic grooved substrate is about 145.8 K in our previous study,[9] which is much larger than that in this study. The reason for this is that the statistical region for the nucleation temperature in the previous study includes the region clinging to the substrate surface, where the temperature is high. On the basis of the nucleation position, the statistical region for the nucleation temperature in the present study is more reasonable than that in our previous study.

For an activated process, the barrier crossing rate is related to the mean first-passage time (MFPT).[31] MFPT has been conducted to obtain the essential parameters of bubble nucleation in our previous study,[16] and the details will not be repeated here. It can be found that the trend of MFPT will reach a platform with a value of τ_J, from which an approximate nucleation rate can be obtained. Figure 11 illustrates the trends of MFPT in cases with different substrates. The MFPT reaches a platform quickly after bubble nucleation for all cases. Therefore, the approximate nucleation rates of 5.77×10^{-5}, 7.25×10^{-5}, and 8.56×10^{-5} $ns^{-1} \cdot nm^{-3}$ are obtained for the liquids on the ideally smooth substrate, grooved substrate, and convex nanostructure substrate, respectively. Obviously, the nucleation rates of liquid on nanostructure substrates are much higher than that on the smooth substrate, which is qualitatively consistent with the conclusions of nucleate boiling experiments showing that the nanostructure substrate can improve the nucleation efficiency.[32]

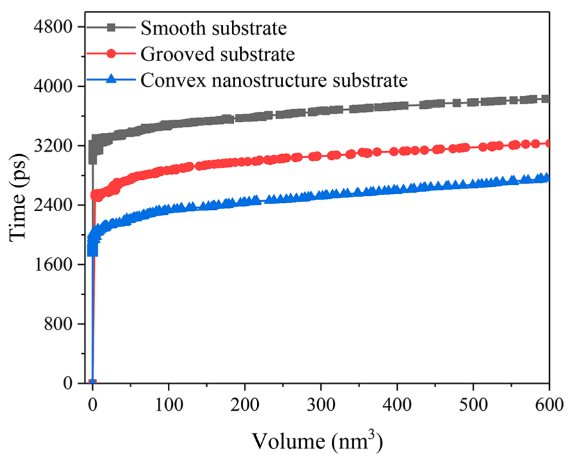

Figure 11. Trends of MFPT in cases with different substrates.

In summary, there are no significant differences between ideally smooth and nanostructure substrates in terms of the nucleation temperature, similar to the experimental conclusions of Stefanović and Novaković. However, the bubble nucleation position is related to nanostructures, which also improve the nucleation rate because of their large exchange area of thermal energy.

CONCLUSIONS

Bubble nucleation on different hydrophilic substrates is investigated by the molecular dynamics simulation method. The feasibility of nucleation on an ideally smooth substrate is verified, and the intrinsic mechanism is revealed by the evolution of atomic energy. Moreover, comparisons in bubble nucleation are made between ideally smooth and nanostructure substrates. The following conclusions can be drawn:

(1) A visible bubble nucleus successfully turns up on an ideally smooth substrate with an unpredicted position. The thermal energy obtained by liquid atoms is nonuniform due to their irregular distribution and movement. Therefore, local liquid atoms near the substrate surface absorb enough thermal energy and overcome their potential barrier at some moment, causing the emergence of a bubble nucleus.

(2) There is no significant difference between nanostructure and ideally smooth substrates in terms of nucleation temperature. The distance between the substrate surface and the nucleation position is longer than the cutoff radius of the potential calculation. Therefore, the substrate geometry has few effects on the initial potential barrier for bubble nucleation, leading to little difference in the required temperature (kinetic energy) of inception nucleation on different substrates.

(3) Compared to the smooth substrate, nanostructure substrates help to promote bubble nucleation. The nanostructure does not provide a nucleation embryo, but affords a large heat transfer area. Liquid atoms near it obtain more kinetic energy to quickly overcome the potential barrier, leading to a high nucleation rate.

AUTHOR INFORMATION

Corresponding Author

Bo Yu − *School of Mechanical Engineering, Beijing Key Laboratory of Pipeline Critical Technology and Equipment for Deepwater Oil & Gas Development, Beijing Institute of Petrochemical Technology, Beijing 102617, P. R. China;* orcid.org/0000-0002-4231-6914; Phone: +86-10-81292805; Email: yubobox@vip.163.com

Authors

Yu-Jie Chen − *Key Laboratory of Thermo-Fluid Science and Engineering of MOE, School of Energy and Power Engineering, Xi'an Jiaotong University, Xi'an Shaanxi 710049, P. R. China*

Xue-Jiao Chen − *Beijing Institute of Aerospace Testing Technology, Beijing 100074, P. R. China;* orcid.org/0000-0002-0197-3918

Yu Zou − *School of Mechanical Engineering, Beijing Key Laboratory of Pipeline Critical Technology and Equipment for Deepwater Oil & Gas Development, Beijing Institute of Petrochemical Technology, Beijing 102617, P. R. China*

Wen-Quan Tao − *Key Laboratory of Thermo-Fluid Science and Engineering of MOE, School of Energy and Power Engineering, Xi'an Jiaotong University, Xi'an Shaanxi 710049, P. R. China;* orcid.org/0000-0002-2348-6299

Complete contact information is available at: https://pubs.acs.org/10.1021/acs.langmuir.0c02832

Notes

The authors declare no competing financial interest.

ACKNOWLEDGMENTS

This work is supported by the National Natural Science Foundation of China (No.51936001, No. 51636006), the Program of Great Wall Scholar (No. CIT&TCD20180313), and the Project for Young Talents of the China National Nuclear Corporation.

REFERENCES

(1) Ilić, M. M.; Petrović, M. M.; Stevanović, V. D. Boiling heat transfer modelling: a review and future prospectus. *Therm. Sci.* **2019**, *23*, 87−107.

(2) Qi, Y.; Klausner, J. F. Comparison of nucleation site density for pool boiling and gas nucleation. *J. Heat Transfer* **2006**, *128*, 13−20.

(3) Bon, B.; Guan, C. K.; Klausner, J. F. Heterogeneous nucleation on ultra smooth surfaces. *Exp. Therm. Fluid Sci.* **2011**, *35*, 746−752.

(4) Chen, T.; Klausner, J. F.; Garimella, S. V.; Chung, J. N. Subcooled Boiling Incipience on a highly smooth microheater. *Int. J. Heat Mass Transfer* **2006**, *49*, 4399−4406.
(5) Ling, K.; Tao, W. Numerical simulation of nucleate boiling in shallow liquid. *Comput. Fluids* **2018**, *164*, 35−40.
(6) Fang, W.; Chen, L.; Kang, Q. J.; Tao, W. Lattice Boltzmann modeling of pool boiling with large liquid-gas density ratio. *Int. J. Therm. Sci.* **2017**, *114*, 172−183.
(7) Yamamoto, T.; Matsumoto, M. Initial stage of nucleate boiling: molecular dynamics investigation. *J. Therm. Sci. Technol.* **2012**, *7*, 334−349.
(8) Hens, A.; Agarwal, R.; Biswas, G. Nanoscale study of boiling and evaporation in a liquid Ar film on a Pt heater using molecular dynamics simulation. *Int. J. Heat Mass Transfer* **2014**, *71*, 303−312.
(9) Chen, Y.; Li, J.; Yu, B.; Sun, D.; Zou, Y.; Han, D. Nanoscale study of bubble nucleation on a cavity substrate using molecular dynamics simulation. *Langmuir* **2018**, *34*, 14234−14248.
(10) Shavik, S. M.; Hasan, M. N.; Morshed, A. K. M. M.; Islam, M. Q. Molecular dynamics study of effect of different wetting conditions on evaporation and rapid boiling of ultra-thin argon layer over platinum surface. *Procedia Eng.* **2015**, *105*, 446−451.
(11) Mao, Y.; Zhang, Y. Molecular dynamics simulation on rapid boiling of water on a hot copper plate. ASME 2013 Heat Transfer Summer Conference collocated with the ASME 2013 7th International Conference on Energy Sustainability and the ASME 2013 11th International Conference on Fuel Cell Science. *Engineering and Technology.* **2014**, *62* (2), 607−612.
(12) Zhou, W.; Li, Y.; Li, M.; Wei, J.; Tao, W. Bubble nucleation over patterned surfaces with different wettabilities: Molecular dynamics investigation. *Int. J. Heat Mass Transfer* **2019**, *136*, 1−9.
(13) Mukherjee, S.; Datta, S.; Kumar Das, A. Molecular dynamic study of boiling heat transfer over structured surfaces. *J. Heat Transfer* **2018**, *140* (5), 054503.
(14) Zhang, L.-Y.; Xu, J.- L.; Lei, J.-P. Molecular dynamics study of bubble nucleation on a nanoscale. *Acta Phys. Sin.* **2018**, *67* (23), 234702.
(15) Chen, Y.; Zou, Y.; Wang, Y.; Han, D.; Yu, B. Bubble nucleation on various surfaces with inhomogeneous interface wettability based on molecular dynamics simulation. *Int. Commun. Heat Mass Transfer* **2018**, *98*, 135−142.
(16) Chen, Y.; Yu, B.; Zou, Y.; Chen, B.; Tao, W. Molecular dynamics studies of bubble nucleation on a grooved substrate. *Int. J. Heat Mass Transfer* **2020**, *158*, 119850.
(17) Liu, Y.; Zhang, X. Molecular dynamics simulation of nanobubble nucleation on rough surfaces. *J. Chem. Phys.* **2017**, *146* (16), 164704.
(18) She, X.; Shedd, T. A.; Lindeman, B.; Yin, Y.; Zhang, X. Bubble formation on solid surface with a cavity based on molecular dynamics simulation. *Int. J. Heat Mass Transfer* **2016**, *95*, 278−287.
(19) Nagayama, G.; Tsuruta, T.; Cheng, P. Molecular dynamics simulation on bubble formation in a nanochannel. *Int. J. Heat Mass Transfer* **2006**, *49*, 4437−4443.
(20) Delhommelle, J.; Millie, P. Inadequacy of the Lorentz-Berthelot combining rules for accurate predictions of equilibrium properties by molecular simulation. *Mol. Phys.* **2001**, *99*, 619−625.
(21) Plimpton, S. Fast parallel algorithms for short-range molecular dynamics. *J. Comput. Phys.* **1995**, *117* (1), 1−19.
(22) Stukowski, A. Visualization and analysis of atomistic simulation data with ovito-the open visualization tool. *Modell. Simul. Mater. Sci. Eng.* **2010**, *18*, 015012.
(23) Shen, V. K.; Debenedetti, P. G. A kinetic theory of homogeneous bubble nucleation. *J. Chem. Phys.* **2003**, *118*, 768−782.
(24) Plesset, M. S.; Zwick, S. A. Growth of vapor bubbles in superheated liquids. *J. Appl. Phys.* **1954**, *25*, 493−500.
(25) Novaković, M.; Stefanović, M. Boiling from a mercury surface. *Int. J. Heat Mass Transfer* **1964**, *7*, 801−807.
(26) Stefanović, M.; Afgan, N. Liquid superheat for vapour formation with and without presence of solid surface. *Desalination* **1972**, *10*, 17−26.
(27) Bankoff, S. G. Entrapment of gas in the spreading of liquid over a rough surface. *AIChE J.* **1958**, *4*, 24−26.
(28) Dhir, V. K. Boiling heat transfer. *Annu. Rev. Fluid Mech.* **1998**, *30*, 365−401.
(29) Barthau, G. Active nucleation site density and pool boiling heat transfer-an experimental study. *Int. J. Heat Mass Transfer* **1992**, *35*, 271−278.
(30) Wang, C. H.; Dhir, V. K. On the gas entrapment and nucleation site density during pool boiling of saturated water. *J. Heat Transfer* **1993**, *115*, 670−79.
(31) Wedekind, J.; Strey, R.; Reguera, D. New method to analyze simulations of activated processes. *J. Chem. Phys.* **2007**, *126*, 134103.
(32) Mehralizadeh, A.; Reza Shabanian, S.; Bakeri, G. Effect of modified surfaces on bubble dynamics and pool boiling heat transfer enhancement: A review. *Therm. Sci. Eng. Prog.* **2020**, *15*, 100451.